Biocatalysis and Agricultural Biotechnology 20 (2019) 101243

Contents lists available at ScienceDirect

Biocatalysis and Agricultural Biotechnology

journal homepage: www.elsevier.com/locate/bab

Acalypha wilkesiana flowers: Phenolic profiling, cytotoxic activity of their biosynthesized silver nanoparticles and molecular docking study for its constituents as Topoisomerase-I inhibitors

Mohamed A. El Raey[a], Ali M. El-Hagrassi[a], Abeer F. Osman[b], Khaled M. Darwish[c], Mahmoud Emam[a,*]

[a] Phytochemistry and Plant Systematics Department, National Research Centre, 33 El Bohouth St., Dokki, P.O. 12622, Giza, Egypt
[b] Department of Chemistry of Natural Compounds, National Research Centre, Dokki, Giza, Egypt
[c] Medicinal Chemistry Department, Faculty of Pharmacy, Suez Canal University, Ismailia, Egypt

ARTICLE INFO

Keywords:
Acalypha wilkesiana flowers
Cytotoxic activity
Green synthesis AgNPs
Molecular docking
Phenolics
Topoisomerase-I.

ABSTRACT

The bio potential behavior of green silver nanoparticles (AgNPs) using *Acalypha wilkesiana* flowers extract weas evaluated. The AgNPs formed were confirmed using surface plasmon resonance band showed in UV–vis spectrophotometer that characterized with spherical shape in size range from 5 to 45 nm depending on Transmission electron microscopy (TEM) and with good stability (−50.75 mV) depending on Zeta-potential measurements. In order to identify the capping agents responsible for the reduction of silver ion and the stabilization of nanoparticles prepared, Fourier transform-infrared spectroscopy (FTIR) and HPLC-ESI-MS analysis were used. Our AgNPs exhibited cytotoxic activity against MCF-7 (Breast carcinoma), PC-3 (Prostate carcinoma) and BJ-1 (skin normal human) cell lines with IC_{50} values 4.00, 3.6 and 4.1 μg/mL, respectively (i.e. the higher selectivity of AgNPs toward prostate than breast cancer cell lines was observed). These highly cytotoxic activity may be back to the presence of the bi-apigenin derivatives; amentoflavone and Cupressuflavone that displayed unique binding docking score towards the active site of human DNA topoisomerase enzyme. The present study is a distinctive application for the biosynthesis of silver nanoparticles in a fast, simple, easy, eco-friendly, inexpensive and effective way.

1. Introduction

Cancer is abnormal propagation of an uncontrolled division of cells that usually invade and destroy the normal cells (Sisodiya, 2013). It is considered a major problem in both developed and developing countries. Every year millions of people are diagnosed with cancer and that leading to death with annual record from 2 to 3% (Kaur et al., 2011). In addition to, the side effects of chemo and radio therapy were recorded, many alternative and/or complementary agents are demanded (Kaur et al., 2011).

Natural compounds derived from plants have been considered as a remarkable prevention or inhibition agents against carcinogenesis. As the cancer preventive agents derived from plants should be developed depending on the selective activity against cancer molecular targets and a new improved structures over time (Kaur et al., 2011; Meyer et al., 1996; Xin et al., 2017; Sivalokanathan et al., 2005).

Topoisomerases targets have been focused for the treatment of certain diseases such as anticancer drugs that act to inhibit these enzymes by blocking the reaction that reseals the breaks in the DNA (Vos et al., 2011). TOP-1 inhibitors represent promising leads for the development of novel cancer chemotherapeutics (Pommier et al., 2010; Pommier, 2009, 2013) especially, from the natural sources that have low toxicity (Xin et al., 2017).

Recently, silver nanoparticles (AgNPs) have introduced in various fields that play a significant role in the biological applications and medicine due to its attractive physiochemical properties (Zayed et al., 2012). AgNPs have found to possess a wide biological activities and cytotoxicity against cancer cells (Elumalai et al., 2010; Safaepour et al., 2009; Kalishwaralal et al., 2010), which makes them vital. The use of plant extracts for synthesis of nanoparticles is potentially advantageous over microorganisms due to the ease of scale up, the less biohazard, and elaborate process of maintaining cell culture (Emam et al., 2017; Marrez et al., 2017).

Acalypha genus (family Euphorbiaceae) consist with about 450

* Corresponding author.
E-mail address: Mahmoudemamhegazy2020@gmail.com (M. Emam).

https://doi.org/10.1016/j.bcab.2019.101243
Received 17 April 2019; Received in revised form 7 July 2019; Accepted 9 July 2019
Available online 10 July 2019
1878-8181/

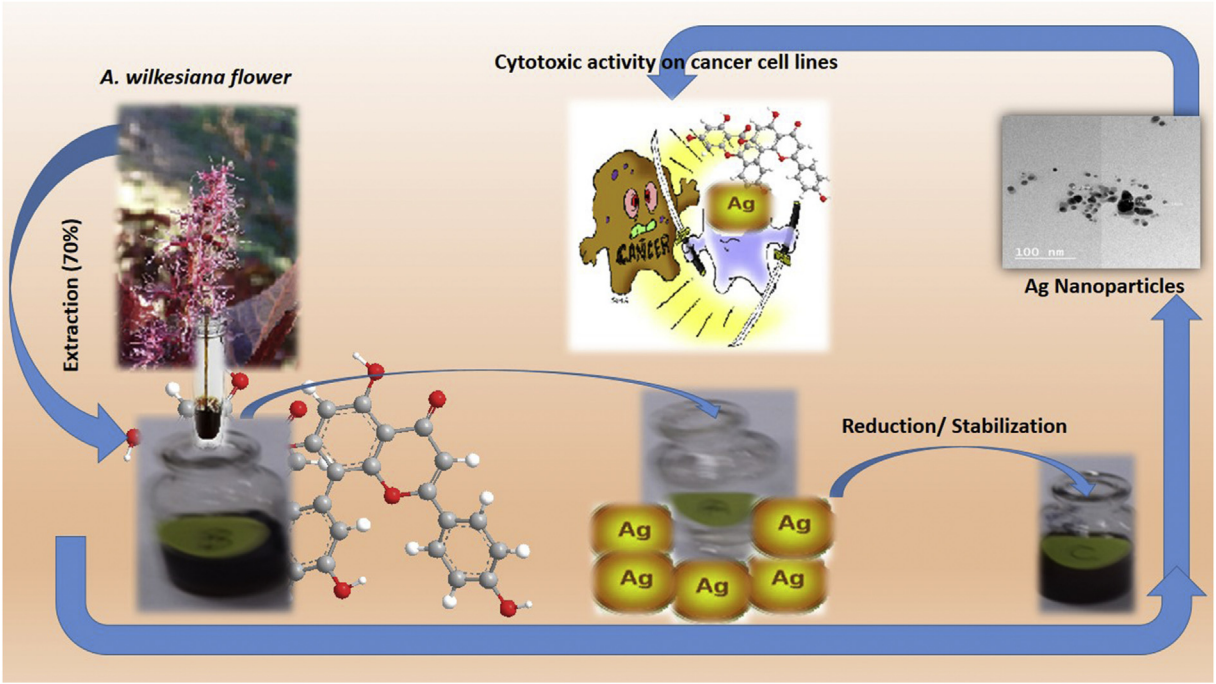

Scheme 1. The bio-synthesis of AgNPs using *A. wilkesiana* flower extract.

species (Webster, 1994). The plant was used traditionally (Akinyemi et al., 2005) and possessed different biological activities (Anokwuru et al., 2015), because of the existence of terpenoids, polyphenols, saponins, and anthraquinones (Adesina et al., 2000). In addition, the plant is widely distributed in Egypt.

The aims of the current study were to prepare the green silver nanoparticles (AgNPs) using *A. wilkesiana* flowers extract and evaluate its cytotoxic activity against cancer cell lines (Breast carcinoma and Prostate carcinoma). As well as, the phenolic profile of *A. wilkesiana* flower extract using HPLC/ESI/MS and the molecular docking as a powerful tool of prediction, simulation and virtual screening of the identified compounds on human DNA topoisomerase enzyme (TOP-I) were studied. To best of our knowledge, this study on these part of the selected plant was not evaluated before. (see Scheme 1)

2. Material and methods

2.1. Materials

Silver nitrate ($AgNO_3$, Merck), Methanol (HPLC, SD Fine-Chem Limited), Dimethylsulphoxide (DMSO, Sigma Aldrich Chemical Co.), Human tumor cell lines (MCF-7 and PC-3, ATCC, Minisota, U.S.A.) and skin normal human cell line (BJ-1) normal skin fibroblast cell line. The tumor cell lines were maintained at the National Cancer Institute, Cairo, Egypt, by serial sub-culturing.

2.2. Collection and identification of plant

Acalypha wilkesiana flower were collected from Egypt (private garden at Giza) in September 2016. The taxonomical features were confirmed by herbarium of Phytochemistry and plant systematic department, Pharmaceutical industries research division, National Research Centre, Dokki, Cairo, Egypt (CAIRC) (M-109).

2.3. Plant extracts preparation

The macerated plant flowers (45 g) were extracted three times with 70% methanol/water (*v:v*). The solvent was evaporated and the dried hydro-alcoholic extract was defatted with petroleum ether. The extract filtered and dried, then stored at 4 °C and used for further experiments.

2.4. HPLC-PDA-MS/MS

HPLC-PDA-MS/MS analysis were done using a Thermo Finnigan LC system (Thermo Electron Corporation, Austin, TX, USA). A Zorbax Eclipse XDB-C18, Rapid resolution, 150 × 4.6 mm, 3.5 µm column was used (Agilent, Santa Clara, CA, USA). A gradient consists of water and acetonitrile (ACN), each having 0.1% formic acid, was applied and acetonitrile was increased from 5 to 30% within 60 min in 1 mL/min flow rate and a 1:1 split before the ESI source. The sample was injected using autosampler. LCQ-Duo ion trap having a Thermo Quest ESI source was used for MS analysis. Xcalibur software (Xcalibur™ 2.0.7, Thermo Scientific, Waltham, MA, USA) was used to control the system. MS operating parameters in the negative mode were used as described before (Sobeh et al., 2017).

2.5. Bio-synthesis of AgNPs

AgNPs were prepared by the reduction of aqueous $AgNO_3$ solution with different concentration of *A. Wilkisiona* extract at room temperature. The mixture was hand shaken and allowed to stand in the dark at room temperature. To study the effect of extract quantity on Ag NPs synthesis, the quantity was varied from 100 µL to 400 µL per 10 mL of silver nitrate solution (1 mM). The concentration of the $AgNO_3$ was still constant over the process (1 mM), while the extract concentration changed, to investigate its effect upon the reduction, size of the bio-synthesized nanoparticles. The obtained nanoparticle solution was purified by repeated centrifugation at 10,000 rpm for 20 min followed by redispersion of the pellet in deionized water. This process was repeated twice to isolate the pure AgNPs and exclude the presence of any unbound plant extract residue or silver nitrate (Emam et al., 2017; Marrez et al., 2017).

2.6. Characterization of the bio-synthesized AgNPs

The UV–vis spectra measurements were recorded using UV-2401

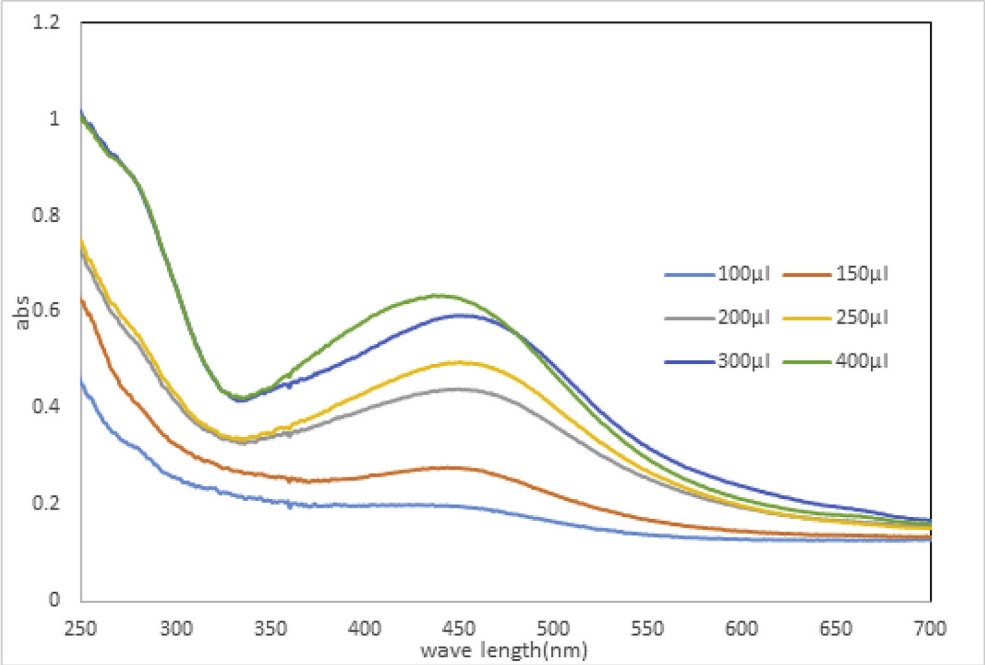

Fig. 1. The SPR band of Ag nanoparticles recorded by UV–vis spectra as a function of varying addition of *A. wilkesiana.*

(PC)S, UV–Vis recording spectrophotometer (Shimadzu, Japan). A FT/IR 6100 spectrometer (Jasco, Japan) was employed to demonstrate the chemical nature of the bio-synthesized Nano-materials in the range of 4000–400 cm^{-1}. The shape and sizes of the as-prepared samples were performed using transmission electron microscope (TEM) (JEOL-JEM-1011, Japan). Zeta potential of the prepared sample was measured, using Nicomp™ 380 ZLS size analyzer, USA. Leaser light scattering was used at 18° for zeta potential measurement.

2.7. Evaluation of cytotoxic activity on human cancer cell line and selectivity index (SI)

The cytotoxicity was carried out using Sulphorhodamine-B (SRB) assay following the method reported by Vichai and Kirtikara (2006) (Vichai and Kirtikara, 2006). SRB is a bright pink aminoxanthrene dye with two sulphonic groups. It is a protein stain that binds to the amino groups of intracellular proteins under mildly acidic conditions to provide a sensitive index of cellular protein content. Samples were prepared by dissolving 1:1 Stock solution and stored at −20 °C in dimethylsulfoxide (DMSO) at 100 mM. Different concentrations of the drug were used 5, 12.5, 25, 50 µg/mL. The percentage of cell survival was calculated as follows:

Surviving fraction = O.D. (treated cells)/ O.D. (control cells)

The IC_{50} values (the concentrations of resveratrol required to produce 50% inhibition of cell growth) were also calculated.

Selectivity Index (SI): the selectivity index (SI) indicates the cytotoxic selectivity (i.e. safety) of the crude extract against cancer cells versus normal cells (BJ-1, skin human normal cell line)(Prayong et al., 2008).

SI = IC_{50} of plant extract in a normal cell line/ IC_{50} of the same plant extract in cancer cell line

2.8. Molecular docking studies

All the ligands were built and energy-minimized using Merck Molecular Force Fields (MMFF) charges and the MMFF force field as implemented in Sybyl X.1 with 2000 steps of the conjugate gradient method to a gradient of 0.001 kcal/Å (Cheng et al., 2000). The obtained minimized were then saved as MDB (Molecular Data Base) file to be used within the molecular docking protocol. The Molecular Operating Environment (MOE) Suite V.2014.09 software was used for docking of the minimized ligands into the binding pocket of the X-ray crystal structure of Human Topoisomerase I-DNA (TOP-1/DNA) ternary covalent complex (PDB ID: 1t8i) (Moe, 2014; Staker et al., 2005). The biological target, obtained from RCSB-Protein data bank, was loaded into the MOE software as to prepare through 3D-protonation as well as autocorrection for atoms types, connections, and charges. The binding site was defined by MOE Alpha Site Finder where selection of the active site involved the crucial catalytic residues and intercalating DNA bases being reported within current literature. Dummy atoms were created from the obtained alpha spheres as the hydrophobic-polar descriptors for the defined TOP-1/DNA active site.

The MOE induced-fit docking protocol was adopted where ligand conformations were generated with the bond rotation method, placed in the site with the triangle matcher method, and ranked with the London dG scoring function. The retained number of poses (set for 10 poses) were then passed to the Refinement, for energy minimization in the pocket, before rescoring with the Generalized Born solvation model/Weighted Surface Area (GBVI/WSA) dG forcefield-based scoring function. The GBVI/WSA dG depends on coulombic electrostatic using the currently loaded charges, protein-ligand van der Waals score, solvation electrostatic, and surface area weighted by exposure (Vilar et al., 2008). The root-mean-square deviation (RMSD) values were considered as a way to assess the validity of the docking protocol keeping the cut-off below 2.0 Å. PyMol v2.0.6 was used for analyzing and visually investigating the ligand-protein interactions of the obtained docking poses (PyMOL).

3. Results and discussion

3.1. Characterisation of biosynthesized AgNPs

3.1.1. UV–vis spectroscopic studies

Ag nanoparticle dispersions are characterized with their brilliant colors and the appearance of the yellowish brown color in the reaction

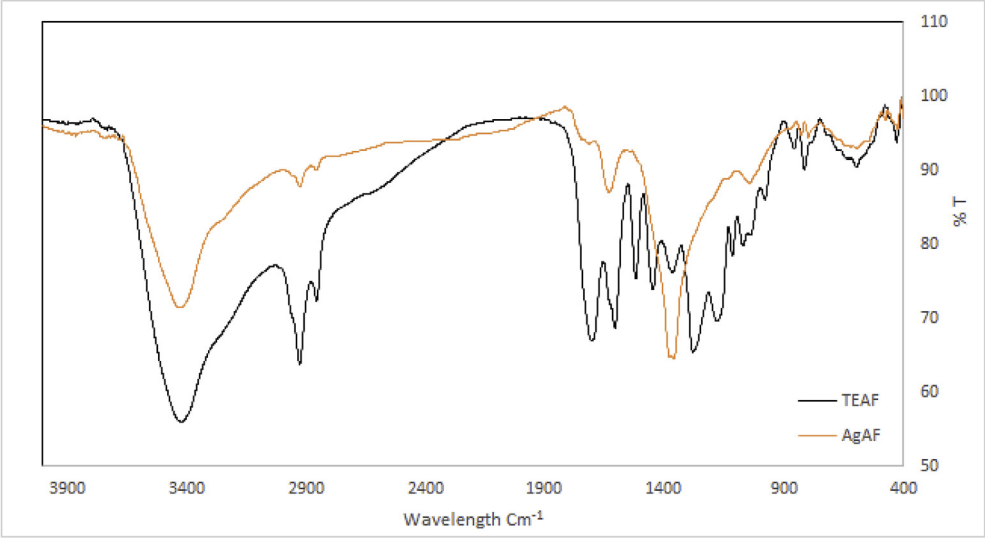

Fig. 2. FTIR spectra of extract stabilized Ag nanoparticles as compared with that of naked *A. wilkesiana Flowers* extract.

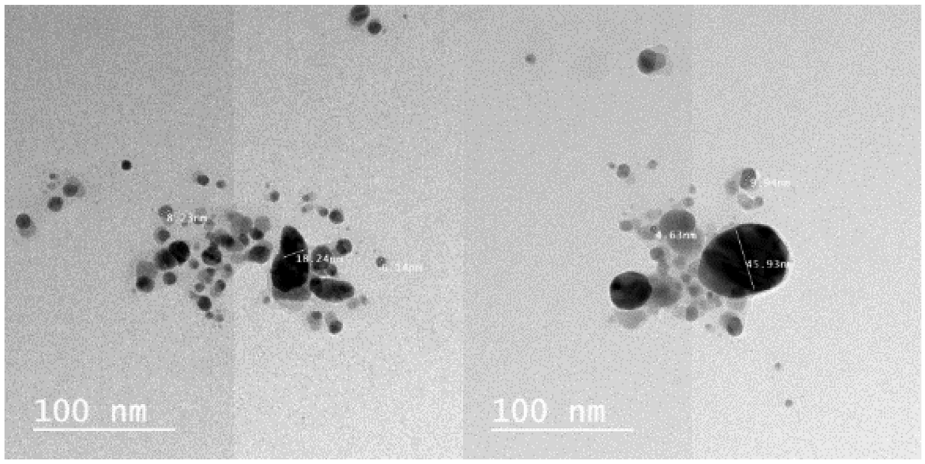

Fig. 3. The TEM images of *A. wilkesiana.* Stabilized Ag nanoparticles at 300 µL.

mixture as an evident for the formation of Ag nanoparticles, due to the surface plasmon resonance (SPR) (Rivero et al., 2013). Fig. 1 illustrates the UV–vis spectra of Ag nanoparticles prepared by adding different amounts of *A. Wilkesiana* to 10 mL of 10^{-3} M $AgNO_3$ solution. The prepared samples show an absorption in the visible region at 444–462 nm due to the SPR band. The intensity of the SPR band grows with increasing *A. Wilkesiana* concentration. The increasing intensity of the SPR band indicates that more Ag^+ ions are reduced to Ag nanoparticles (Zayed et al., 2015). The previous studies suggested that the gradually blue shift to shorter wavelengths at UV–vis spectra after adding 400 µL of extract might be attributed to the shape of nano particles become more spherical (Chakraborty, 1998; Baia et al., 2006).

3.1.2. FTIR spectra analysis

The active functional groups of the total *Acalypha flower* extract (TAFE) were qualitatively evaluated using FTIR spectroscopy as given in Fig. 2. The broad and strong IR peak at 3420 cm^{-1} was attributed to the stretching vibrations of (–OH) group of alcoholic/phenolic compounds. After the interaction with Ag^{1+} ions, this IR band was slightly shifted to 3427 cm^{-1}. The vibrational bands at 1703 and 1606 cm^{-1} in the extract spectrum were assigned as the stretching of –C═O and N–H bending (Babarinde et al., 2012).

Upon the reduction of Ag nanoparticles, these two bands suffered from broadening and weakening and were shifted to 1711 and 1623 cm^{-1}. The vibrational peaks at 1517 cm^{-1} (aromatic ring) (Zayed et al., 2019), 1447 cm^{-1} (–O–H bending), 1279 cm^{-1} (C–O stretching) of the extract, were completely disappeared after biosynthesis of Ag nanoparticles. The FTIR analysis of the Acalypha spectrum indicated remarkable structural changes in the absorption peak frequencies. This is attributed to the fact that the interaction with the metal ions causes shift in the peaks frequencies. These observed shifts in IR bands indicated that there were Ag binding/reduction processes occur on the functional groups of the extract. The FTIR analysis displayed the presence of ionizable functional groups such as (O–H, NH2, C–O, C═O) which have the ability to interact with Ag^{1+} ions (Zayed et al., 2012, 2015; Emam et al., 2017). Therefore, these functional groups are responsible for the reduction and/or protection of Ag nanoparticles.

3.1.3. TEM studies

The shape and size of the as-prepared Ag nanoparticles are evaluated using the HRTEM technique. Fig. 3 displays the TEM image of the particle distribution of the prepared Ag nanoparticles. It can be seen that the as-prepared nanoparticles are mainly spherical in shape with particle size varies between 5 and 45 nm. The particles are separated from each other which reflect the capping action of the plant extract in the preparation process.

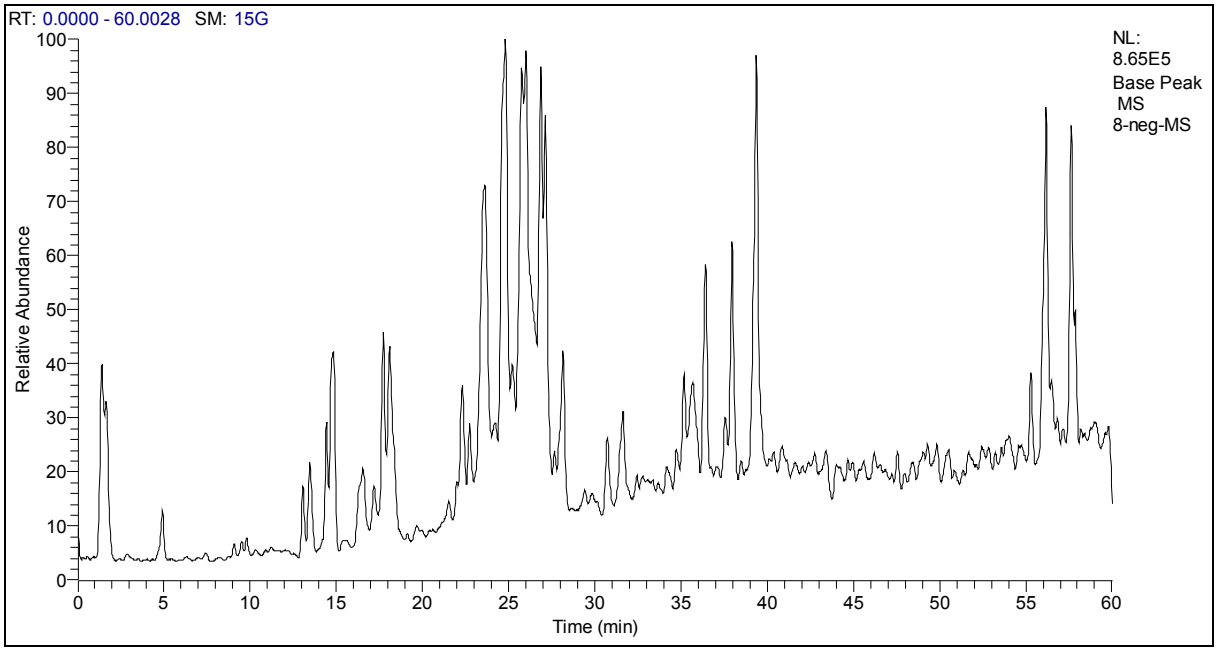

Fig. 4. Base beak chromatogram of *A. wilkesiana* flowers methanolic extract.

Table 1
Phenolic profile of identified metabolites.

Peak	Proposed structure	tR	[M-H]-	MS2(m/z)	References
1	Monogallyol glucose	4.90	331	169	Ramirez et al. (2013)
2	5- caffeoyl quinic acid	9.09	353	179, 191	An et al. (2013)
3	3-caffeoyl quinic acid	9.53	353	179, 191	An et al. (2013)
4	4- caffeoyl quinic acid	9.80	353	179, 191	An et al. (2013)
5	feruloylquinic acid I	10.68	367	191, 193	Kuhnert et al. (2010)
6	Brevifolin carboxylic acid	13.07	291	247	Santos et al. (2013)
7	Brevifolin carboxylic acid dev. (Brocchlin carboxylic acid)	14.71	291	217, 233, 247	Hawas (2007)
8	methyl gallic acid	16.52	183	169, 125	Ramirez et al. (2013)
9	feruloyl quinic acid II	16.63	367		Kuhnert et al. (2010)
10	Tergallic acid- glucoside	22.03	631	613, 445, 331	Fernandes et al. (2011)
11	Galloyl HHDP gluconic acid	23.00	649	631, 605, 302	Tanaka et al. (1992)
12	DHHDP-HHDP-galloyl glucose I (Geraniin)	24.66	951	933, 631,301	Fischer et al. (2011)
13	DHHDP-HHDP-galloyl glucose II (Granatin B)	25.68	951	933, 631,301	Fischer et al. (2011)
14	DHHDP-HHDP-galloyl glucose III	26.86	951	933, 631,301	Fischer et al. (2011)
15	DHHDP-HHDP-galloyl glucose IV	27.18	951	933, 631,301	Fischer et al. (2011)
16	Unknown	27.95	379	347, 319, 303	
17	Apigenin C-hexoside-C-pentoside [(iso) Schaftoside]	31.67	563	545, 503, 473, 443, 383, 353	
18	Quercetin-3-*O* rhamno hexoside	35.18	609	179, 301, 463	He et al. (2013)
19	Quercetin-3-*O* rhamno hexoside	36.32	609	179,301, 463	He et al. (2013)
20	Kaempferol -3-*O* rhamno hexoside	37.94	593	285, 447	Moco et al. (2006)
21	Kaempferol -3-*O* rhamno hexoside	39.41	593	285, 447	Moco et al. (2006)
22	Bi-Apigenin (Amentoflavone)	55.32	537	375, 399, 417, 443	Liao et al. (2015)
23	Bi-Apigenin (Cupressuflavone)	56.21	537	375, 399, 417, 443	Liao et al. (2015)
24	Bi-Apigenin (Agathiflavone)	57.88	537	375, 399, 417, 443	Liao et al. (2015)

3.1.4. Zeta potential measurement

The zeta potential of the synthesized AgNPs was determined in water as dispersant. The zeta potential of AgNPs was found to be −50.75 mV, indicating the dispersion and good stability. The negative value confirms the repulsion among the particles and thereby the good stability of the colloidal formulation (Varadavenkatesan et al., 2019; Vinayagam et al., 2017).

3.2. Phenolic profile of A. wilkesiana flowers aq. Methanolic extract

HPLC-PDA-MS/MS has been used to identify the polyphenolic content of the total extract of the *A. wilkesiana* flowers. The twenty three phenolic compounds have been identified based on their molecular weights, fragmentation pattern and the spectral data from the PDA detector (Fig. 4). All compounds fragmentations were compared with those published data as shown in (Table 1). Phenolic constituents were investigated and showed different classes of plant polyphenols as shown below.

Cinnamic acid derivatives: Two types of cinnamic acid derivatives were detected and identified as follow: Compounds **2**, **3** and **4** showed $[M-H]^-$ ion at *m/z* 353 with fragments at *m/z* 191; quinic acid moiety and 179; caffeic acid moiety, suggesting compounds **2**, **3** and **4** to be 5-*O*-Caffeoyl quinic acid, 3-*O*-Caffeoyl quinic acid and 4-*O*-Caffeoyl quinic acid, respectively (An et al., 2013). Compounds **5** and **9** showed $[M-H]^-$ ion at *m/z* 367 with fragments at *m/z* 191; quinic acid moiety, suggesting compounds **5** and **9** to be feruloyl quinic acid (Kuhnert et al., 2010). **Gallotannins:** Compound **1**, showed $[M-H]^-$ ion at *m/z* 331 with UV at 270 nm, followed by fragments at *m/z* 169 $[M-H-162]^-$,

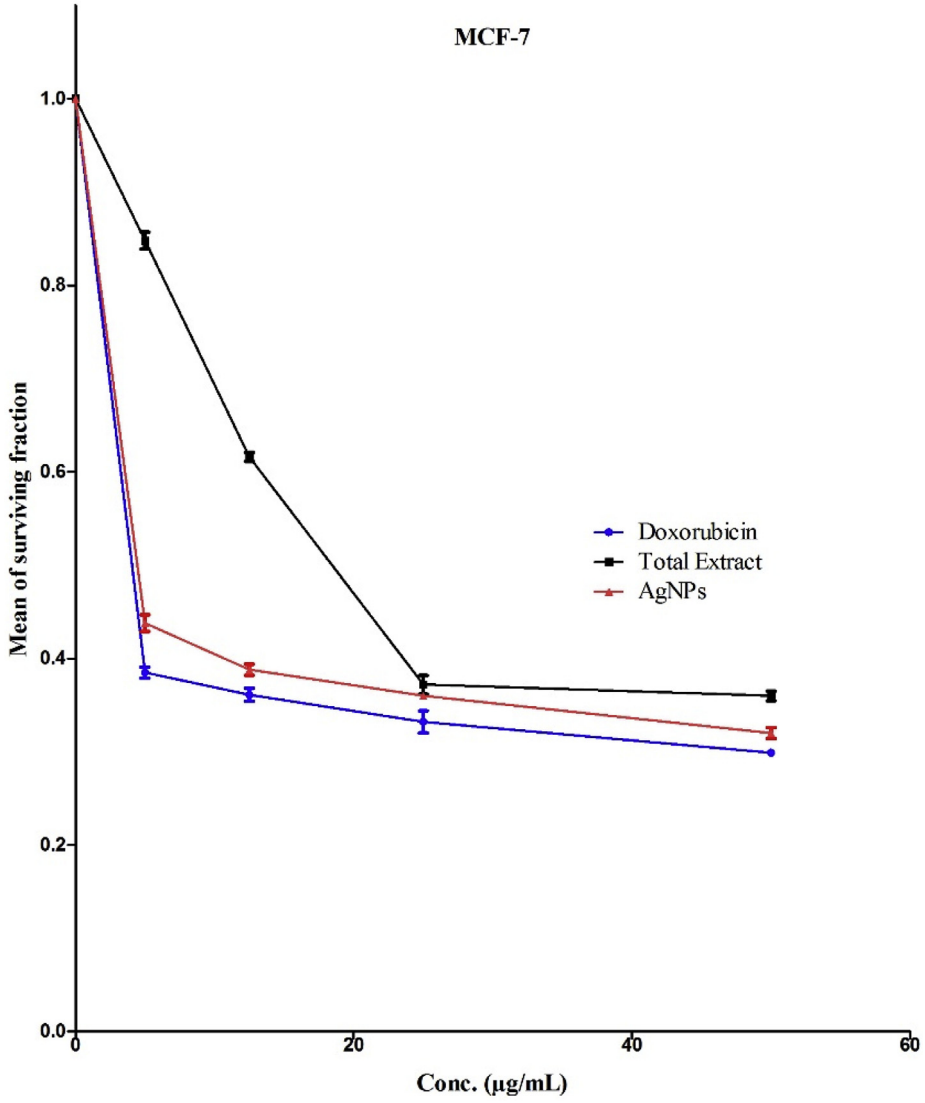

Fig. 5. The effects of different concentrations of the *A. wilkesiana* flower extract and AgNPs against standard doxorubicin on MCF-7 cell survival as assessed through the SRB Cytotoxic Assay. Results are the mean ± SD of three individual studies.

suggesting compound **1** to be monogalloyl glucose (Ramirez et al., 2013). Compound **8**, exhibited $[M-H]^-$ ion at m/z 183 and showed fragments at *m/z* 169 characteristic for gallic acid suggesting compound **8** to be methyl gallate (Ramirez et al., 2013). **Ellagitannins:** *A. wilkesiana* flowers have high and diverse content of ellagitannins. It contains different isomers DHHDP- HHDP- galloyl glucose, these isomers may be granatin B or geraniin which was isolated from the seed (El-Raey et al., 2016). It is obviously showed absence of Galloyl HHDP Glucose which are one the main constituents of the seeds (El-Raey et al., 2016). Compound **10** showed $[M-H]^-$ ion at *m/z* 631 along with fragments at m/z 613 $[M-H-18]^-$ due to loss of one H_2O molecule and formation of dehydrated tergallic acid glycoside, suggesting **10** to be tergallic acid hexoside (Fernandes et al., 2011). Compound **11** showed $[M-H]^-$ ion at *m/z* 649 along with fragments at m/z 631$[M-H-18]^-$ due to loss of one H_2O molecule, In addition to fragment 605 $[M-H-CO_2]^-$, suggesting that 11 to be Galloyl HHDP gluconic acid (Tanaka et al., 1992). Compounds **12**, **13, 14** and **15** showed $[M-H]^-$ ion at *m/z* 951 along with fragments at *m/z* 933 $[M-H-18]^-$ due to loss of one H_2O molecule and 915 due to loss of two water molecules followed by *m/z* 613 due to loss of ellagic acid after two water molecules then it loss gallic acid to show *m/z* 445 and showed also characteristic fragment at *m/z* 301 of ellagic acid. Based on these fragments and comparing of these results with those published data (Fischer et al., 2011). Compounds **12, 13, 14** and **15** are positional isomers and identified to be (galloyl-HHDP-DHHDP-glucose). **Brevifolin carboxlic acids and isomers:** Compounds **6** and **7** showed $[M-H]^-$ ion at *m/z* 291and showed fragments at *m/z* 247 due to loss of CO_2 molecule, suggesting this compounds to be brevifolin carboxylic acid and its positional isomer Brocchlin carboxylic acid (Santos et al., 2013; Hawas, 2007). **Flavonoids, Apigenin C-glycoside and biapigenin:** Compound **17** exhibited a molecular ion $[M-H]^-$ ion at *m/z* 563 with daughter ions at 443 and 473$[M-H-90]^-$ which are characteristic for flavone C-glycosides; suggesting **17** to be (iso) schaftoside (Colombo et al., 2008). Compounds **(18, 19) and (20, 21)** showed $[M-H]^-$ ion at *m/z* 609 and 593, respectively. In addition to, MS/MS fragments at *m/z* 463 and 447 $[M-H-146]^-$, respectively due to loss of rhamnosyl moiety and showed characteristic peak for quercetin *m/z* 301, 179 characteristic peaks for kaempferol at *m/z* 285. Suggesting compounds **17** and **18** to be quercetin rhamno hexoside (He et al., 2013) and compounds **19**and **20** kaempferol rhamno hexoside (Moco et al., 2006). Compounds **22, 23 and 24** exhibited $[M-H]^-$ ion at *m/z* 537 and MS/MS fragments at *m/z* 375, 399, 417 and 443, suggested compounds **22, 23 and 24** to be Biapigenin positional isomers e.g amentoflavone, its isomers cupprssoflavone and Agathiflavone (Liao et al., 2015).

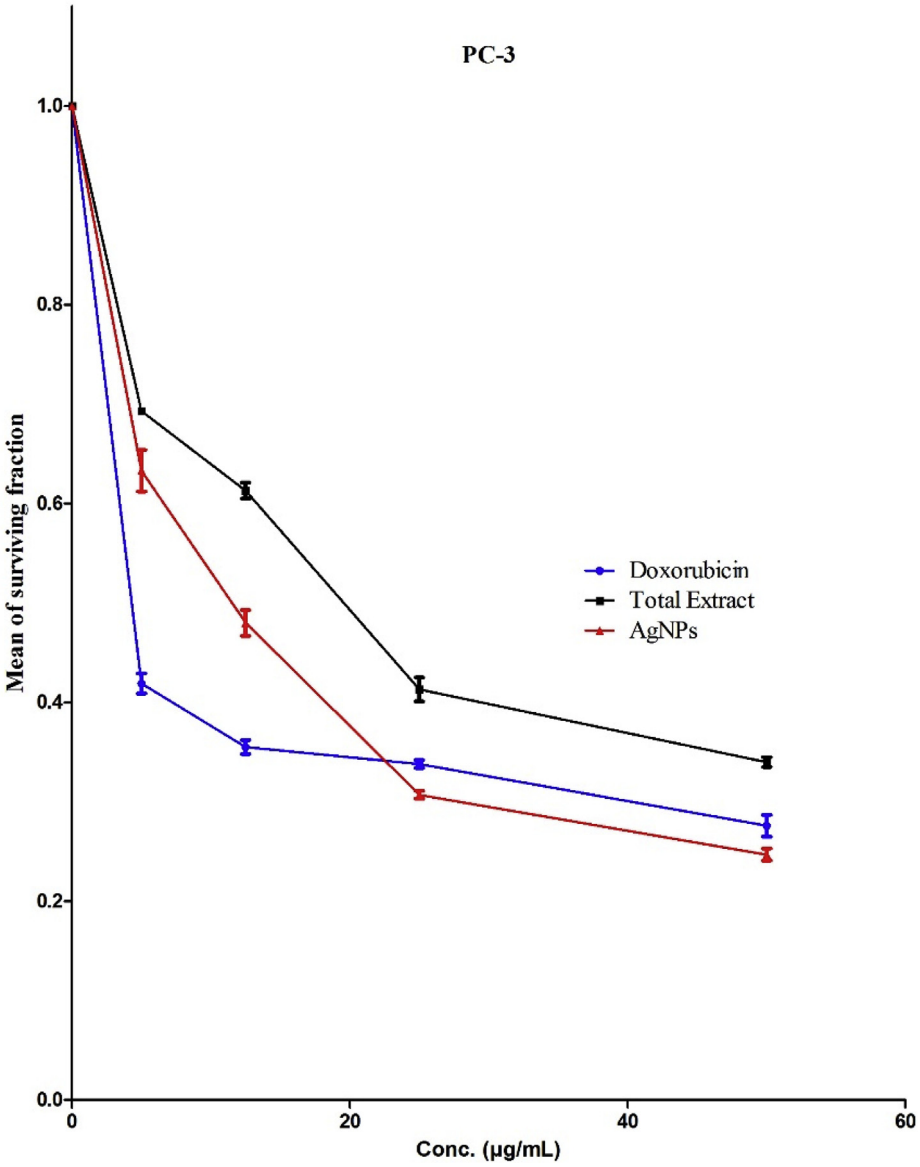

Fig. 6. The effects of different concentrations of the *A. wilkesiana* flower extract and Ag NPs against standard doxorubicin on PC-3 cell survival as assessed through the SRB Cytotoxic Assay. Results are the mean ± SD of three individual studies.

Table 2
IC_{50} of antitumor activity of the total extract, Ag NPs of *A. wilkesiana* flowers and standard doxorubicin on Breast carcinoma cell line (MCF-7) and Prostate carcinoma cell line (PC-3).

IC_{50} (µg/mL) of silver nano particle using *A. Wilkesiana* flower extract against Doxorubicin			
	Ag NPs	Doxorubicin	Total extract
MCF-7	4.00	3.83	18.50
PC-3	3.60	4.28	16.70

3.3. Cytotoxicity assay

The total extract of *A. wilkesiana* and its AgNPs were investigated to evaluate their cytotoxicity effect against both MCF-7 (Breast carcinoma cell line) and PC-3 (Prostate carcinoma cell line) as shown in Figs. 5 and 6, respectively. For the dose response was studied and their IC_{50} values were calculated (Table 2).

Table 2 showed that the *A. wilkesiana* flowers total extract had distinctive cytotoxic activity against Breast carcinoma cell line (MCF-7) and Prostate carcinoma cell line (PC-3) with IC_{50} 18.50 and 16.70, respectively. In addition, the cytotoxic activity of the prepared AgNPs were increased against Breast carcinoma cell line (MCF-7) and Prostate carcinoma cell line (PC-3) with IC_{50} of 4.00 and 3.60, respectively.

Also, the prepared AgNPs using the *A. wilkesiana* flowers extract was subjected to further investigation at lower concentration to calculate their IC_{50} values and explore its cytotoxicity on skin normal human cell line (BJ-1) to evaluate its SI values.

After introducing the prepared AgNPs against BJ-1, the cytotoxic effect was evaluated as 95% at 100 µg/mL with IC_{50} = 4.1 µg/mL. Although, the prepared AgNPs showed high cytotoxicity on both cancer and normal cell lines. But, the selectivity index was detected as 1.03 and 1.14 against MCF-7 and PC-3 cancer cell lines, respectively. Which means that the prepared AgNPs showed a weak selectivity toward cancer cell lines but, the higher selectivity toward prostate cancer cell line than breast cancer cell line (El-Hallouty et al., 2015).

The activity of the total extract of *A. wilkesiana* flowers was attributed to the presence of phenolics that reported with their potential antioxidant activities and their effects to prevent different oxidative

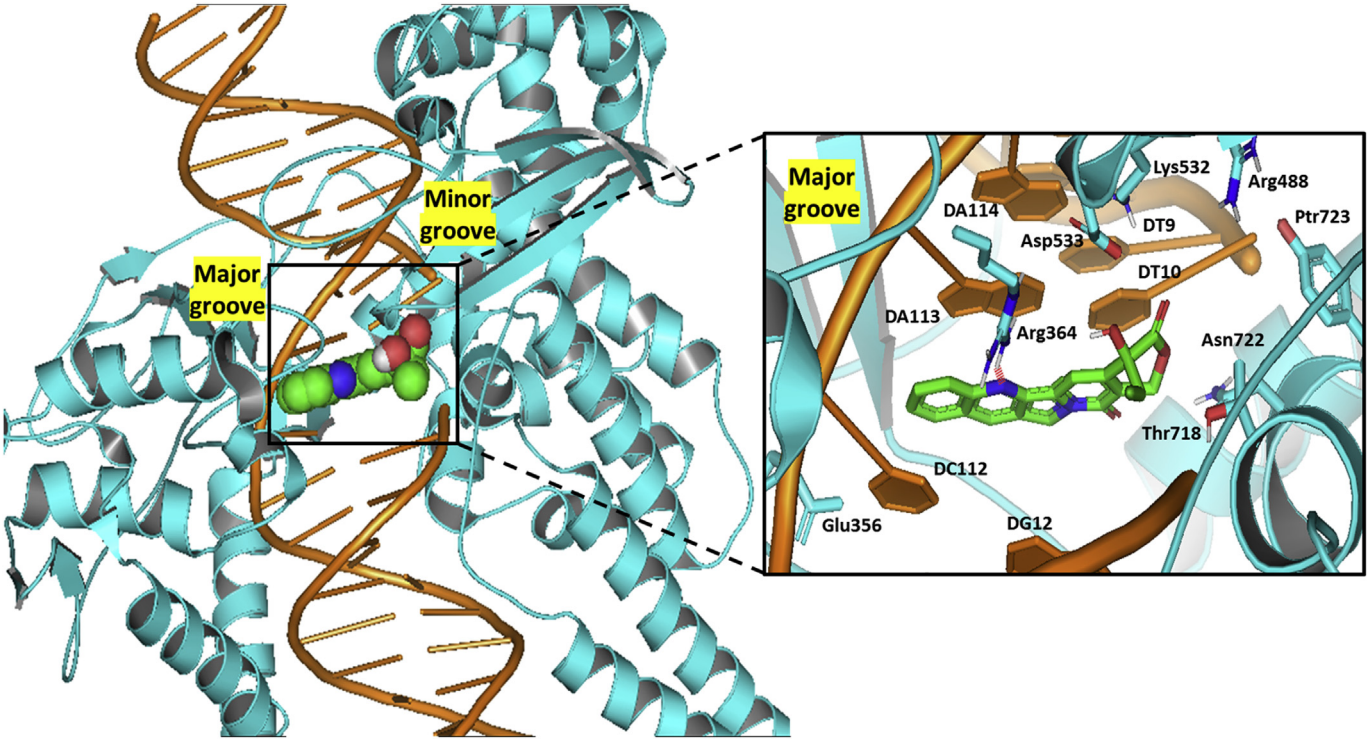

Fig. 7. The architecture of the crystallized human TOP-1/DNA covalent complex active site (PDB ID: 1t8i). The ternary complex is diagrammed with protein (cyan) and DNA (orange) in cartoon 3D-representation, while crystallized ligand, Camptothecin, as spheres (green as carbon, red as oxygen, blue as nitrogen, white as hydrogen). The DNA bases are represented as ladder sticks. The zoomed image is the stereoview of crystallized camptothecin (sticks) occupying the chemically significant active site of the TOP-1/DNA covalent complex adjacent to the scissile DNA strand. Polar interaction (Hydrogen bonding) is depicted as red dashed-lines. Only residues (sticks) located within 4 Å radius of bound ligand are displayed and labeled with sequence number. (For interpretation of the references to color in this figure legend, the reader is referred to the Web version of this article.)

stress diseases such as cancer as well as, their cytotoxic activity (Kavitha et al., 2015; Madlener et al., 2009; Chen et al., 2009; El-Raey et al., 2016; Vassallo et al., 2013; Lee et al., 2012; Shrestha et al., 2012; Andrade et al., 2018). Also, the increasing activity of the prepared AgNPs was attributed to their small particle size with large surface area which facile endocytosis of AgNPs molecules into the nucleus followed by DNA damage and apoptosis (Govindaraju et al., 2015).

3.4. Molecular docking studies

In order to prove the potential observed activity and to study its mechanism, the molecular docking study on human topoisomerase-1 were performed. The total extract of *A. wilkesiana* flowers was tested for its growth inhibitory effect on MCF-7 (Breast carcinoma) and PC-3 (Prostate carcinoma) cell lines by using Sulphorhodamine-B (SRB) assay following the method reported by Vichai and Kirtikara (2006) compared with doxorubicin standard.

Being thrilled with the furnished *in-vitro* cytotoxic activity, a molecular docking outflow has been conducted for selected six polyphenolic compounds identified from the *Acalypha Wilkesiana* flowers extract. Setting the biological target to the Human Topoisomerase I-DNA (TOP-1/DNA) covalent complex (PDB ID: 1t8i) for the *in-silico* studies was rationalized since a plethora of reported naturally-based polyphenolics, including most of our investigated compounds, have been linked to TOP-1/DNA as potential inhibitors (Grynberg et al., 2002; Tomczyk et al., 2008; Xin et al., 2017; El-Kashak et al., 2017; Kumar Jain et al., 2017).

Generally, TOP-1 is a pivotal enzyme that functions to relax positive supercoiled DNA throughout replication, transcription, or even mitosis. The latter biological function is conducted through DNA cleavage, followed by controlled strand rotation, and finally resealing (Vos et al., 2011). Being highly expressed in a number of human solid tumors, TOP-1 inhibitors represent promising leads for the development of novel cancer chemotherapeutics (Pommier et al., 2010). Most of the natural-existing TOP-1 poisons stabilize the TOP-1/DNA covalent complexes by inhibiting the religation step of a single-strand nick, generating DNA lesions and ultimately induces apoptosis (Pommier et al., 2010; Pommier, 2009, 2013).

Within the current literature, the two investigated biflavonoids, agathisflavone and amentoflavone, have been assessed for their inhibitory effects on TOP-1/DNA via the decatenation and relaxation assays, where only the band corresponding to the supercoiled DNA was observed at the drugs' 200 μM concentrations (Grynberg et al., 2002). Additionally, great DNA-binding ability of the neoflavanoid-related compound, brevifolin carboxylic acid, was confirmed by means of the TOP-1/DNA inhibition assay and ethidium displacement assay using the calf thymus DNA (Tomczyk et al., 2008). On the other hand, the polyphenolic ellagitannins and flavonol-based derivatives have exhibited significant activities on human topoisomerase enzymes suggesting their prospective anti-cancer therapeutic application (Auzanneau et al., 2012; López-Lázaro et al., 2000, 2002).

The adopted 3.0 Å X-ray crystal structure of TOP-1/DNA covalent complex (PDB ID: 1t8i) bounds to the plant alkaloid, camptothecin, the prototype natural TOP-1 inhibitor (Fig. 7). Generally, the planar nature of the reported TOP-1 inhibitors allows them to intercalate between DNA base pairs at the site of single-strand cleavage, where the flat planar ring structure is placed on the intact strand side of DNA. Such intercalative binding mode can be augmented by the free electron pair of few ligands on major groove side of intercalation binding pocket being in contact with Arg364, a residue when being mutated confer resistance to camptothecin. Several reported models postulated that further H-bonding between the ligands, DNA bases and catalytic residues, such as Asn352, Lys532, Asp533, Asn722, or Tyr723, could also correlated for further intercalation support (Seng et al., 2010; Staker

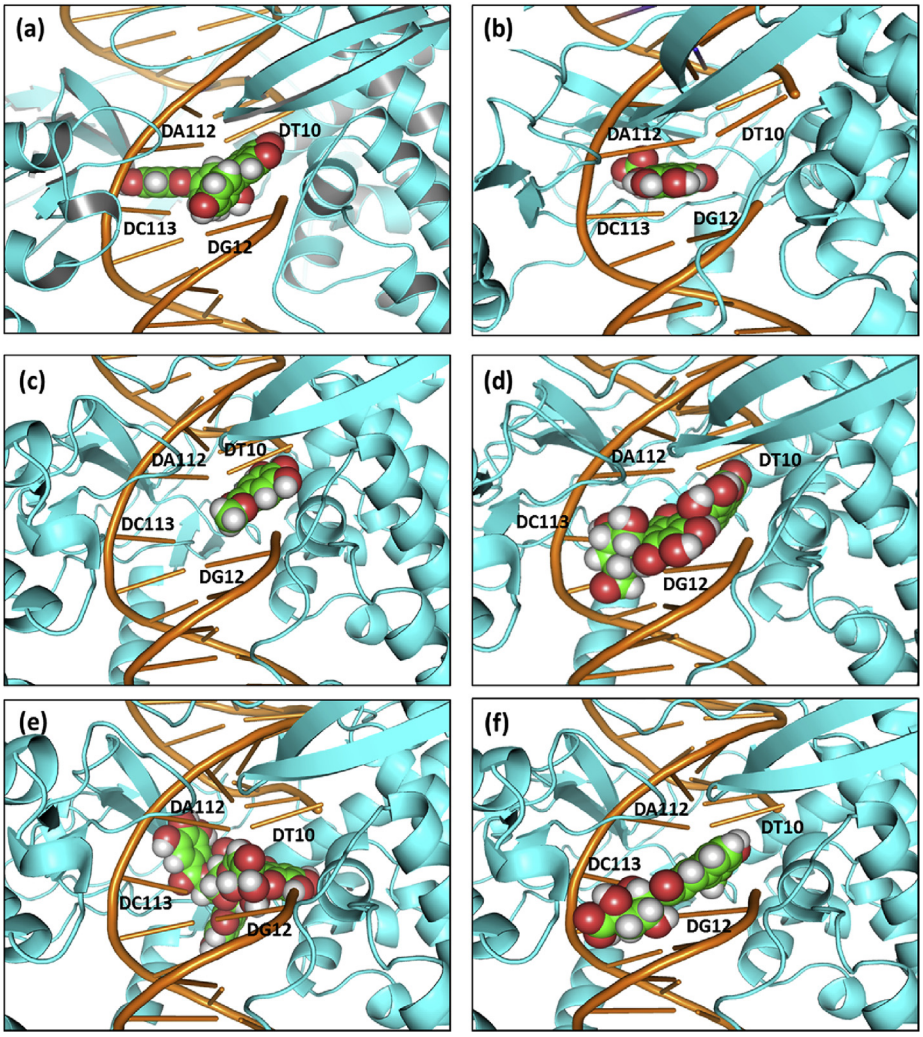

Fig. 8. The predicted binding modes of the investigated compounds, isolated from *Acalypha Wilkisiona*, at the human TOP-1/DNA covalent complex active site (PDB ID: 1t8i); (a) amentoflavone; (b) brevifolin carboxylic acid; (c) methyl gallate; (d) tergallic acid-*C*-glycoside; (e) Granatin B; (f) 4-*O*-feruolylquinic acid. The predicted ternary complex is diagrammed with protein (cyan) and DNA (orange) in cartoon 3D-representation with DNA bases as ladder sticks, while docked ligands as spheres (green as carbon, red as oxygen, blue as nitrogen, white as hydrogen). Only amentoflavone shows extended anti-coplanar conformation favoring excellent occupation within the DNA bases DA112, DC113, DT10, DA12 (ACTA) of the active site. Contrarily, brevifolin carboxylic acid or methyl gallate show restricted intercalation to either DA112, DC113 at the DNA intact strand or D12 at the scissile strand, respectively. (For interpretation of the references to color in this figure legend, the reader is referred to the Web version of this article.)

et al., 2002; Laco et al., 2002; Yousuf et al., 2018).

Throughout our molecular docking studies, the bioflavonoids and 3-*O*-glycosidic flavonols exhibited the highest docking ranks ($S = -8.90$ to -7.80 kcal mol^{-1}) compared with that of other investigated ligands and even the redocked crystallized camptothecin. Such upper-handed scores were for the advent of favored extended planner conformations possessed by the biflavonoids permitting their optimum placement within the DNA base pairs at the Topo I active site (Fig. 8a). Although, both neoflavonoids predicted highly extensive intercalation supports through interactions with any of the DNA bases (DT-10, DC-112, DA-113) and catalytic residues (Glu356, Arg364, Lys425, Asn722) (Table 3). Such interactions could not excel their docking scoring energies, which could be reasoned for the small-sized neoflavonoid skeleton permitting a limited occupation of the intercalation binding pocket (Fig. 8b). Similar observation was predicted for the small-sized methylated gallic acid derivatives, where these gallotannin-hydrolyzed end products are oriented within a concise space near the sessile DNA strand exhibiting the modest docking scores (Fig. 8c).

Interestingly, the bioflavonoids exhibited anti-coplanar conformations due to the rotation around the single bonds separating the two flavone scaffolds in a way to minimize the steric clashes between the substituted hydroxyl groups. This additional treat of non-planar topography causes the bioflavonoids to further extend within the active site achieving more extended occupacy within the DNA bases (DA112, DC113, DT10, DG12 = ACTG) that can be correlated with the high docking scores. The latter correlation can be confirmed with the tergallic acid-*C*-glycoside binding mode which confers limited anti-coplanarity between the fused tetracyclic ring and gallic acid moiety, the thing that furnish an intermediate docking score (-7.59 kcal mol^{-1}) (Fig. 8d).

Concerning the highly extended conformation of ellagitannin-based analogues (Granatin B and lagerstannin C), the gallic acids and fluorene-like moieties have been oriented towards the non-scissile and scissile DNA strands, respectively. Nevertheless, moderate docking scores were assigned for both ligands (-7.0271 and -6.7511 kcal mol^{-1}) which could be correlated to the highly flexible central scaffold connecting the two moieties together. Such flexible central core is suggested for the inability to conserve the favored extended anti-coplanar conformations within the crucial DNA bases (ACTG) as being illustrated for Granatin B (Fig. 8e). Despite the relatively restricted conformation of the cinnamic acid conjugated enone linker, the quinic acid ester derivatives (4 or 3-*O*-feruloyl- and caffeoylquinic acid) fail to adopt the favored intercalating orientation towards the DA112 and DC113 at the intact DNA strand (Fig. 8f).

Extensive investigation of the predicted binding mode for each ligand showed that both biflavonoids depicted optimum intercalation with favored supporting polar or π-π and π-hydrogen interactions with the catalytic residue or DNA bases of both the scissile and non-scissile strands (Table 3). Such observations confer the excelling scoring energies of amentoflavone and cupressuflavone. Notably, the central benzopyrone ring of all biflavonoids are predicted to be posed towards the cleaved DNA single-strand. While as, the free lone electrons of the heteroxyclic pyrone ring showed great proximity towards the Arg364 (3.1-to-4.5 Å) on the major groove side of intercalation binding pocket

Table 3
The Data of Ligand-Docking Studies on human TOP-1/DNA covalent complex.

Ligand name	MOE docking Scores (*S*) [a] (Kcal moL^{-1})	RMSD [b] (Å)	Ligand-target interaction description [Type; Length (Å); Angle (°); Binding Residues]
Camptothecin (Redocked)	−5.94	1.71	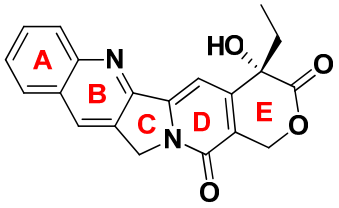 Hydrogen bonding ; 2.24 Å ; 122° ; Arg-364 (=N**H**$_2^+$) with ring **B** (**N**) acceptor π-π stacking ; 3.40 Å ; DC112 with ring **A** π-π stacking ; 3.40 Å ; DA113 with ring **A** π-π stacking ; 3.51 Å ; DA113 with ring **B**
Amentoflavone	−8.90	1.92	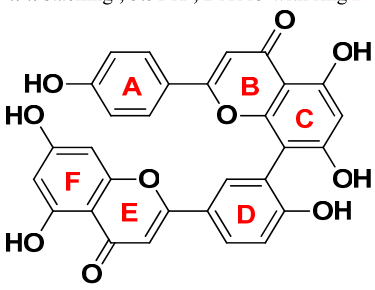 Hydrogen bonding ; 2.6 Å ; 149.9° ; DG12 (Sugar **O**) with ring **D** (O**H**) donor π-Cation interaction ; 4.44 Å ; Arg364 (=N**H**$_2^+$) with ring **A** π-Hydrogen interaction ; 3.15 Å ; DG12 with ring **D** (O**H**) π-Hydrogen interaction ; 2.76 Å ; DG12 with ring **D** (**H**) π-π stacking ; 3.92 Å ; DC112 with ring **F**
Cupressuflavone	−8.08	1.29	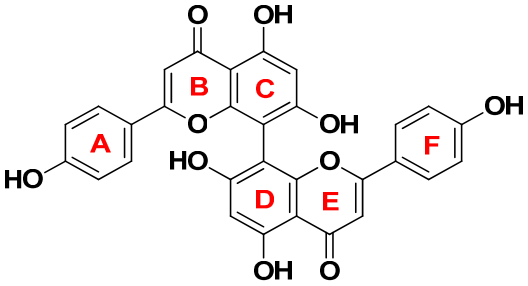 Hydrogen bonding ; 3.06 Å ; 127.8 ° ; Arg364 (=N**H**$_2^+$) with ring **B** (C=**O**) acceptor Hydrogen bonding ; 2.71 Å ; 133.8 ° ; Arg364 (NH**H**) with ring **C** (**O**H) acceptor Hydrogen bonding ; 2.20 Å ; 146.3 ° ; Arg364 (NH**H**) with ring **C** (**O**H) acceptor Hydrogen bonding ; 2.71 Å ; 145.2 ° ; DC112 (NH**H**) with ring **D** (**O**H) acceptor
Agathisflavone	−7.80	1.10	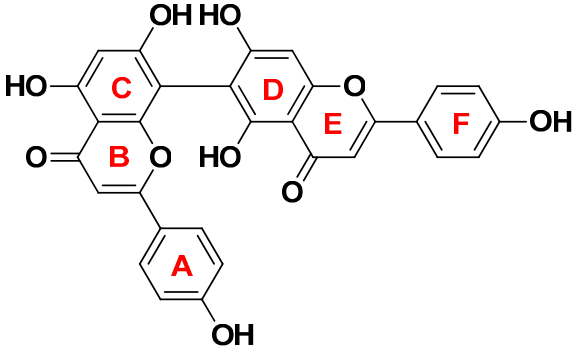 Hydrogen bonding ; 3.31 Å ; 111.6 ° ; Thr718 (**O**H) with ring **C** (O**H**) donor π-Hydrogen interaction ; 3.71 Å ; DG12 (**H**) with ring **A**

(*continued on next page*)

Table 3 (*continued*)

Ligand name	MOE docking Scores (*S*) [a] (Kcal moL^{-1})	RMSD [b] (Å)	Ligand-target interaction description [Type; Length (Å); Angle (°); Binding Residues]
Tergallic acid-*C*-glycoside	−7.60	1.47	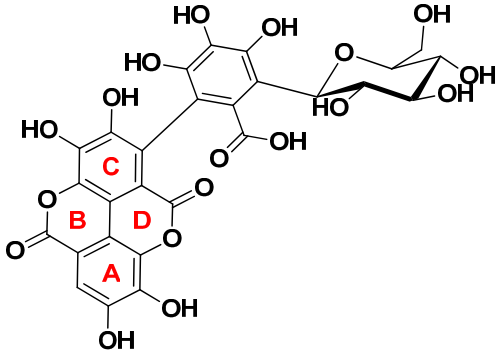 Ionic bonding ; 3.26 Å ; 128.9 ° ; Arg364 (=N**H**$_2^+$) with Gallic acid (C=O(**O**$^-$)) Hydrogen bonding ; 1.90 Å ; 149.8 ° ; Arg364 (NH**H**) with Sugar ring (-**O**H) Hydrogen bonding ; 2.70 Å ; 128.3 ° ; Asn722 (C=**O**) with ring **A** (O**H**) donor Hydrogen bonding ; 2.70 Å ; 159 ° ; DG12 (NH**H**) with Sugar ring (O) acceptor
Brocchlin carboxylic acid	−5.82	1.50	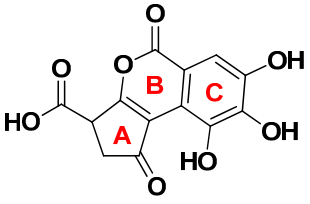 Hydrogen bonding ; 2.92 Å ; 151.9 ° ; Arg364 (=N**H**$_2^+$) with ring **A** (C=**O**) acceptor Hydrogen bonding ; 2.01 Å ; 166.9 ° ; Asn722 (C=**O**) with ring **C** (O**H**) donor Hydrogen bonding ; 2.60 Å ; 132.9 ° ; Asn352 (NH**H**) with (C=**O**(OH)) acceptor Hydrogen bonding ; 2.30 Å ; 158 ° ; DC112 (NH**H**) with (C=O(**O**H)) acceptor π-Hydrogen interaction ; 4.12 Å ; DA113 with ring **A** (CH-**H**) π-π stacking ; 3.69 Å ; DT10 with ring **C**
Brevifolin carboxylic acid	−5.67	0.33	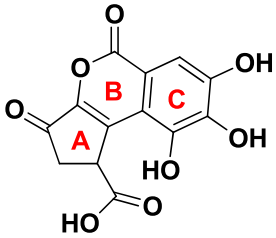 Hydrogen bonding ; 2.57 Å ; 144.0 ° ; Glu356 (C=O**O**$^-$) with ring **A** (O**H**) donor Hydrogen bonding ; 1.9 Å ; 153 ° ; Lys425 (=N**H**$_3^+$) with ring **A** (C=**O**(OH)) acceptor Hydrogen bonding ; 2.30 Å ; 142.1 ° ; Arg364 (=N**H**$_2^+$) with ring **C** (O**H**) donor π-π stacking ; 3.78 Å ; DA113 with ring **C** π-π stacking ; 3.50 Å ; DC112 with ring **C**

(*continued on next page*)

Table 3 (*continued*)

Ligand name	MOE docking Scores (*S*) [a] (Kcal moL^{-1})	RMSD [b] (Å)	Ligand-target interaction description [Type; Length (Å); Angle (°); Binding Residues]
Kaempferol-3-*O*-rutinoside	−8.01	1.62	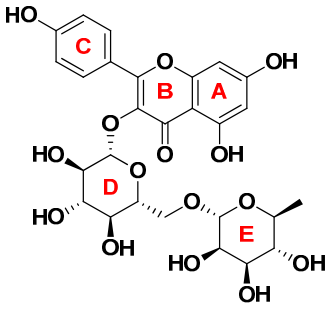 Hydrogen bonding ; 2.16 Å ; 111.2 ° ; Gly365 (-N**H**, backbone) with Sugar **E** (**O**H) acceptor Hydrogen bonding ; 2.46 Å ; 141.2 ° ; Arg364 (-NH**H**) with Sugar **A** (**O**H) acceptor Hydrogen bonding ; 2.29 Å ; 141.8 ° ; His632 (N**H**) with ring **C** (**O**H) acceptor Hydrogen bonding ; 2.19 Å ; 145.8 ° ; DC112 (C=**O**, base) with ring **A** (O**H**) donor Hydrogen bonding ; 1.38 Å ; 133.8 ° ; DG12 (Sugar **O**) with ring **D** (O**H**) donor π-Hydrogen interaction ; 3.33 Å ; DG12 (-P-O**H**, backbone) with ring **C**
Rutin (Quercetin-3-*O*-rhamno hexoside)	−8.31	1.48	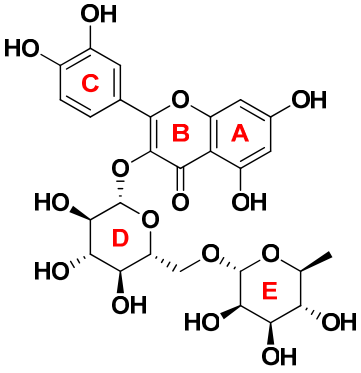 Hydrogen bonding ; 2.12 Å ; 107.6 ° ; Lys751 (=NH**H**) with Sugar **E** (**O**H) acceptor Hydrogen bonding ; 2.18 Å ; 153.6 ° ; DC112 (-NH**H**, base) with Sugar **D** (**O**H) acceptor π-π Stacking ; 4.10 Å ; DG12 with ring **C**
Schaftoside	−7.93	1.89	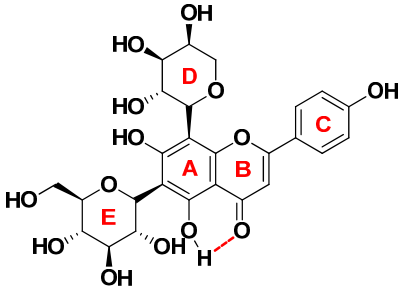 Hydrogen bonding ; 2.03 Å ; 105.6 ° ; Asp533 (-COO**H**) with Sugar ring **E** (O**H**) donor Hydrogen bonding ; 2.02 Å ; 150.0 ° ; Tyr426 (-C=**O**, backbone) with ring **C** (O**H**) donor Intramolecular Hydrogen interaction ; 1.84 Å ; 136.8 ° ; Flavonol C=**O** with O**H**

(*continued on next page*)

Table 3 (*continued*)

Ligand name	MOE docking Scores (*S*) [a] (Kcal moL^{-1})	RMSD [b] (Å)	Ligand-target interaction description [Type; Length (Å); Angle (°); Binding Residues]
Granatin B	−7.03	0.89	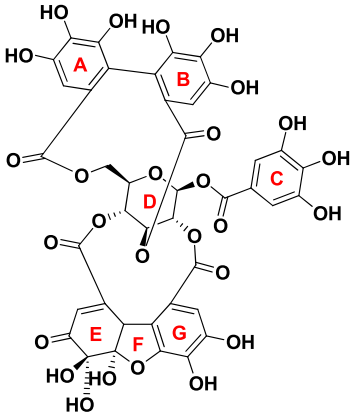 Hydrogen bonding ; 2.22 Å ; 119.2 ° ; Tyr426 (-C=**O**, backbone) with ring **B** (O**H**) donor Hydrogen bonding ; 1.64 Å ; 136.5 ° ; Lys425 (-NH**H**) with ring **A** (**O**H) acceptor Hydrogen bonding ; 1.98 Å ; 125.8 ° ; Asn722 (-C=**O**) with ring **G** (O**H**) donor Hydrogen bonding ; 2.34 Å ; 87.9 ° ; DG12 (**P**-OH) with ring **G** (O**H**) donor π-Hydrogen interaction ; 1.97 Å ; DG12 with ring **F** (O**H**)
Lagerstannin C	−6.75	1.73	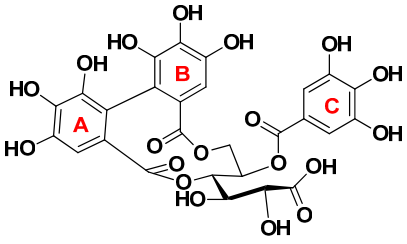 Hydrogen bonding ; 3.13 Å ; 101.9 ° ; DG12 (**3-O**, ribose) with linear hydroxylated hexanoic acid (O**H**) donor
4-*O*-methyl gallic acid	−4.12	1.59	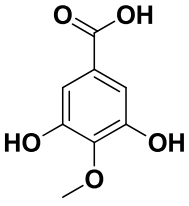 Hydrogen bonding ; 1.93 Å ; 141.3 ° ; Asp533 (-CO**O**-) with Gallic acid (COO**H**) donor π-Hydrogen interaction ; 3.00 Å ; DG12 (-P-O**H**, backbone) with Gallic acid ring
3-*O*-methyl gallic acid	−4.47	1.77	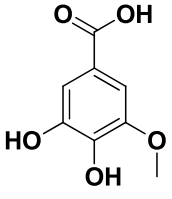 Hydrogen bonding ; 2.22 Å ; 123.0 ° ; His632 (-NH**H**) with Gallic acid (C**O**OH) acceptor π-Hydrogen interaction ; 3.36 Å ; DG12 (-P-O**H**, backbone) with Gallic acid ring

(*continued on next page*)

Table 3 (*continued*)

Ligand name	MOE docking Scores (*S*) [a] (Kcal moL^{-1})	RMSD [b] (Å)	Ligand-target interaction description [Type; Length (Å); Angle (°); Binding Residues]
4-*O*-Feruolylquinic acid	−6.32	1.20	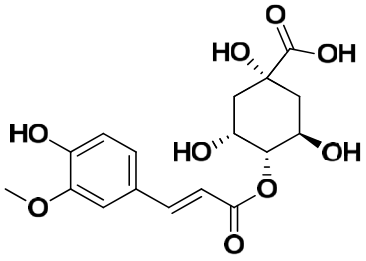 Hydrogen bonding ; 2.32 **Å** ; 140.2 **°** ; Asp533 (-COO**H**) with Cinnamic acid (O**H**) donor Hydrogen bonding ; 2.30 **Å** ; 142.8 **°** ; DC112 (Ribose **O**$_1$) with Quinic acid (O**H**) donor van der Waals interaction ; 4.28 **Å** ; DG12 (Purine Base) with Cinnamic acid (O**CH**$_3$) π-Hydrogen interaction ; 4.15 **Å** ; DG12 (Sugar **H**C**5**) with Cinnamic acid ring
3-*O*-Feruolylquinic acid	−6.15	1.38	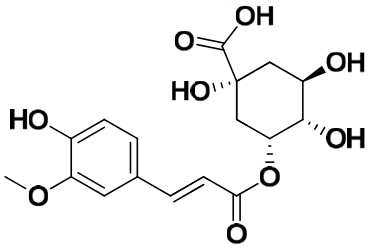 Hydrogen bonding ; 2.16 **Å** ; 144.4 **°** ; Asp533 (-COO**H**) with Cinnamic acid (O**H**) donor Hydrogen bonding ; 2.26 **Å** ; 132.4 **°** ; Gly363 (C=**O**, backbone) with Quinic (COO**H**) donor Hydrogen bonding ; 3.28 **Å** ; 120.6 **°** ; DG12 (-NH**H**) with Quinic acid (**O**H) acceptor
4-*O*-Caffeoylquinic acid	−5.74	2.00	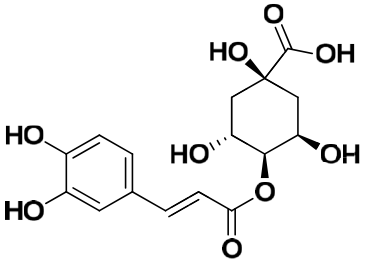 Hydrogen bonding ; 2.03 **Å** ; 123.4 **°** ; Asp533 (-COO**H**) with Cinnamic acid (O**H**) donor Hydrogen bonding ; 2.22 **Å** ; 115.1 **°** ; Gly363 (C=**O**, backbone) with Quinic acid (O**H**) donor
3-*O*-Caffeoylquinic acid	−5.22	1.61	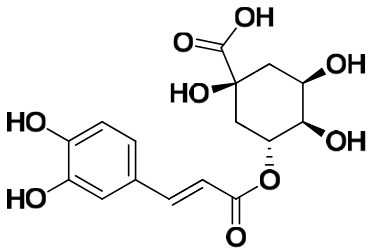 Hydrogen interaction ; 2.27 **Å** ; 143.8 **°** ; DG12 (-NH**H**) with Quinic acid (**O**H) π-Hydrogen interaction ; 3.52 **Å** ; DG12 (-P-O**H**, backbone) with Cinnamic acid ring

(*continued on next page*)

Table 3 (*continued*)

Ligand name	MOE docking Scores (*S*) [a] (Kcal moL^{-1})	RMSD [b] (Å)	Ligand-target interaction description [Type; Length (Å); Angle (°); Binding Residues]
Monogalloyl glucose	−6.44	1.36	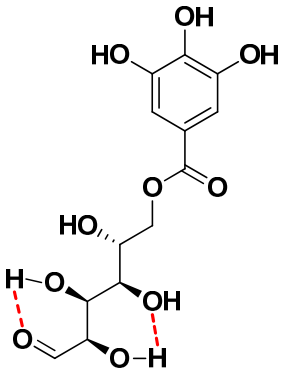 Hydrogen interaction; 2.12 Å; 112.6°; Asp533 (-C=O, backbone) with Gallic (OH) donor Hydrogen interaction; 1.99 Å; 144.6°; His632 (-NH, backbone) with Gallic (OH) acceptor Hydrogen interaction; 2.03 Å; 122.6°; Lys532 (OH) with Gallic acid (OH & C=O) donors Hydrogen interaction; 2.46 Å; 122.9°; Arg488 (=N^{+}HH) with Gallic acid (-COOH) acceptor Intramolecular Hydrogen interaction ; 2.23 Å ; 125.4 ° ; Sugar -C=O with OH Intramolecular Hydrogen interaction ; 2.07 Å ; 125.1 ° ; Sugar OH with OH

[a] MOE (***S***): scoring function assigned for the best-ranking pose chosen based on visual inspection and after refinement through rescoring by the GBVI/WSA dG scoring function . [b]RMSD: Root mean standard deviation of the best-ranking pose as compared to the crystal.

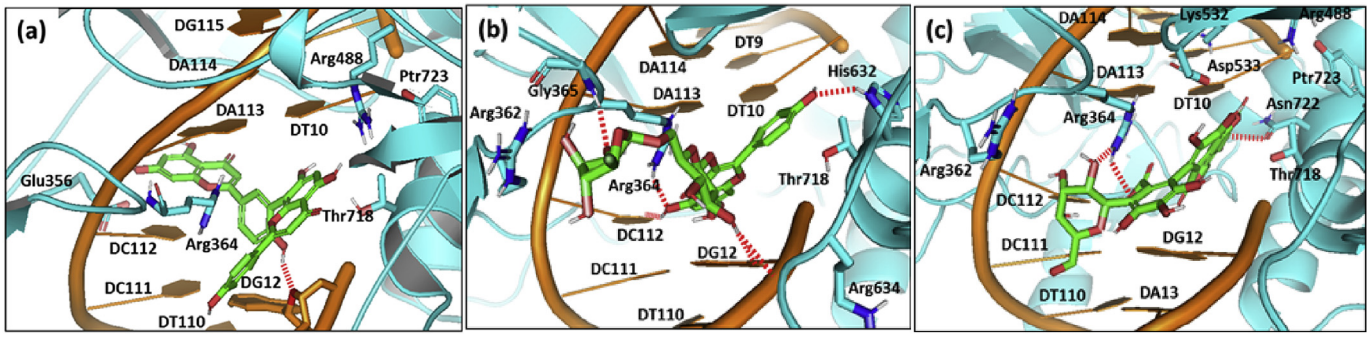

Fig. 9. The predicted docking poses of the investigated compounds, isolated from *Acalypha Wilkisiona*, at the human TOP-1/DNA covalent complex active site (PDB ID: 1t8i); (a) Amentoflavone; (b) kaempferol-3-*O*-rutinoside; (c) tergallic acid-*C*-glycoside. The predicted ternary complex is diagrammed with protein (cyan) and DNA (orange) in cartoon 3D-representation with DNA bases as Flat solid rings, while docked ligands as spheres (green as carbon, red as oxygen, blue as nitrogen, white as hydrogen). Polar interactions (Hydrogen bonding) discussed in text are depicted as red dashed-lines. Only residues located within 4 Å radius of bound ligand are displayed as sticks and labeled with sequence numbers. (For interpretation of the references to color in this figure legend, the reader is referred to the Web version of this article.)

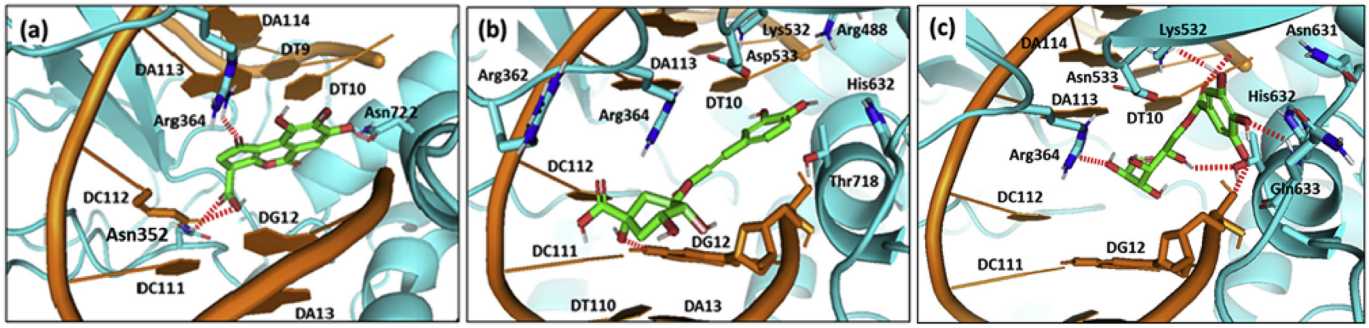

Fig. 10. The predicted docking poses of the investigated compounds, isolated from *Acalypha Wilkisiona*, at the human TOP-1/DNA covalent complex active site (PDB ID: 1t8i); (a) brocchlin carboxylic acid; (b) 3-*O*-caffeoyl-quinic acid; (c) monogalloyl glucose. The predicted ternary complex is diagrammed with protein (cyan) and DNA (orange) in cartoon 3D-representation with DNA bases as Flat solid rings, while docked ligands as spheres (green as carbon, red as oxygen, blue as nitrogen, white as hydrogen). Polar interactions (Hydrogen bonding) discussed in text are depicted as red dashed-lines. Only residues located within 4 Å radius of bound ligand are displayed as sticks and labeled with sequence numbers. (For interpretation of the references to color in this figure legend, the reader is referred to the Web version of this article.)

(Fig. 9a).

Fig. 9b describes the predicted pose of kaempferol-3-*O*-rutinoside, the representative compound of flavonols. The ligand is extended with its phenolic hydroxyl group towards the scissile DNA strand while the terminal sugar part is conferred by favored polar interaction with Gly365 at the intact DNA strand. Further support through π-π and π-hydrogen interactions have been illustrated between the flavonol moiety and both DG12 and DC112. On the other hand, the tergallic acid derivative showed several supporting interactions with Arg364, Asn772, and DG12. Nevertheless, the ligand failed to achieve favored intercalation within the non-scissile strand (between DA112 or DC113) showing its terminal sugar part being protruded out of the active binding site (Fig. 9c).

Moving towards the predicted docking conformations of the neoflavonoid-related compounds, brevifolin carboxylic acid predicted a more concise intercalation towards the non-scissile strand supported by DC112, DA113, Arg364, and Lys425 interactions. On the contrary, brocchlin carboxylic acid exhibited better intercalation with the DT10 (scissile strand) supported with polar interactions with Asn352, Arg364, and Asn772 (Fig. 10a). On similar bases, the four quinic acid ester derivatives showed a more retracted orientation towards the non-scissile strand with their quinic acid scaffolds being solvent exposed and protruded out of the binding site (Fig. 10b). Such orientations furnish comparable docking scores to that of the neoflavonoid-related compounds. Finally, the solely chemical-class related compound, monogalloyl glucose, depicts a concise binding mode to the cleaved DNA strand for the advent of intramolecular hydrogen bonding within the open sugar chain allowing its own self-folding (Fig. 10c).

In conclusion, the previously described differential docking binding modes of our 19 investigated compounds ensures the superiority of binding site occupancy as a significant influence on the predicted docking scores of different ligands. Such favored occupacy is mostly related to preferential for intercalation with the ACTG bases, with more preference for those at the intact strand (DA112 and DC113). Moreover, the favored pattern of supporting polar or hydrophobic interactions with the catalytic residue or DNA bases can serve to efficiently direct the intercalating ligand within the four DNA bases of both the scissile and non-scissile strands.

4. Conclusion

The green synthesis process of the prepared silver nanoparticles were achieved by the direct interaction of silver nitrate with plant extract in aqueous solution without the interference of any external effects. The effect of phenolic concentration was found to play an important role in the preparation of AgNPs as both reducing and stabilizing agents. Silver nanoparticles using *A. wilkisiona* flower extract have great potential selectivity toward prostate carcinoma cell line (PC-3) than breast carcinoma cell line (MCF-7). Also, the virtual studies of the tentative identified phenolic metabolites as Top-I inhibitors showed strong binding energy scores. The docked values are either equal to or exceeding that of the co-crystallized ligand Camptothecin. This might be attributed to the existence of several phenolic (OH) and/or COOH groups in the molecules. *A. wilkisiona* flower extract and its prepared AgNPs could be used in pharmaceutical industry in the future.

Conflicts of interest

There is no conflict of interests.

Acknowledgments

The authors are gratefully thankful to Dr. M. Sobeh (IPMB), Universität Heidelberg, for collecting HPLC-MS/MS data. Also, we wish to thank both Dr. Ahmed A. Hasabo Drug Bioassay-Cell Culture Laboratory, National Research Centre, Egypt for providing the normal cell line and Prof. Dr. Wael H Eisa Spectroscopy Department, National Research Centre, Egypt for his guidance.

References

Adesina, S., Idowu, O., Ogundaini, A., Oladimeji, H., Olugbade, T., Onawunmi, G., Pais, M., 2000. Antimicrobial constituents of the leaves of Acalypha wilkesiana and Acalypha hispida. Phytother Res. 14, 371–374.

Akinyemi, K.O., Oladapo, O., Okwara, C.E., Ibe, C.C., Fasure, K.A., 2005. Screening of crude extracts of six medicinal plants used in south-west Nigerian unorthodox medicine for anti-methicillin resistant Staphylococcus aureus activity. BMC Compl. Altern. Med. 5, 6.

An, H., Wang, H., Lan, Y., Hashi, Y., Chen, S., 2013. Simultaneous qualitative and quantitative analysis of phenolic acids and flavonoids for the quality control of apocynum venetum L. Leaves by hplc–dad–esi–it–tof–ms and hplc–dad. J. Pharm. Biomed. Anal. 85, 295–304.

Andrade, A.W.L., Da Conceição Machado, K., Da Conceição Machado, K., Figueiredo, D.D.R., David, J.M., Islam, M.T., Uddin, S.J., Shilpi, J.A., Costa, J.P., 2018. In vitro antioxidant properties of the biflavonoid agathisflavone. Chem. Cent. J. 12, 75.

Anokwuru, C.P., Sinisi, A., Samie, A., Taglialatela-Scafati, O., 2015. Antibacterial and antioxidant constituents of Acalypha wilkesiana. Nat. Prod. Res. 29, 1180–1183.

Auzanneau, C., Montaudon, D., Jacquet, R., Puyo, S., Pouysegu, L., Deffieux, D., Elkaoukabi-Chaibi, A., De Giorgi, F., Ichas, F., Quideau, S., 2012. The polyphenolic ellagitannin vescalagin acts as a preferential catalytic inhibitor of the A isoform of human dna topoisomerase ii. Mol. Pharmacol. 82, 134–141.

Babarinde, A., Babalola, J.O., Adegoke, J., Osundeko, A.O., Olasehinde, S., Omodehin, A., Nurhe, E., 2012. Biosorption of Ni (ii), Cr (iii), and Co (ii) from solutions using Acalypha hispida leaf: kinetics, equilibrium, and thermodynamics. J. Chem. 2013, 1–8.

Baia, L., Baia, M., Kiefer, W., Popp, J., Simon, S., 2006. Structural and morphological properties of silver nanoparticles–phosphate glass composites. Chem. Phys. 327, 63–69.

Chakraborty, P., 1998. Metal nanoclusters in glasses as non-linear photonic materials. J. Mater. Sci. 33, 2235–2249.

Chen, H.-M., Wu, Y.-C., Chia, Y.-C., Chang, F.-R., Hsu, H.-K., Hsieh, Y.-C., Chen, C.-C., Yuan, S.-S., 2009. Gallic acid, a major component of toona sinensis leaf extracts, contains a ros-mediated anti-cancer activity in human prostate cancer cells. Cancer Lett. 286, 161–171.

Cheng, A., Best, S.A., Merz Jr., K.M., Reynolds, C.H., 2000. Gb/sa water model for the Merck molecular force field (mmff). J. Mol. Graph. Model. 18, 273–282.

Colombo, R., Yariwake, J.H., Mccullagh, M., 2008. Study of C-and O-glycosylflavones in sugarcane extracts using liquid chromatography: exact mass measurement mass spectrometry. J. Braz. Chem. Soc. 19, 483–490.

El-Hallouty, S.M., Fayad, W., Meky, N.H., El-Menshawi, B.S., Wassel, G.M., Hasabo, A.A., 2015. In vitro anticancer activity of some Egyptian plant extracts against different human cancer cell lines. Int. J. Pharmtech Res 8, 267–272.

El-Kashak, W.A., Osman, S.M., Gaara, A.H., El-Toumy, S.A., Mohamed, T.K., Brouard, I., 2017. Phenolic metabolites, biological activities, and isolated compounds of Terminalia muelleri extract. Pharmaceut. Biol. 55, 2277–2284.

El-Raey, M.A., Mohamed, T.K., El-Kashak, W.A., Fayad, W.O., 2016. Phenolic constituents and biological activities of Acalypha wilkesiana forma tricolor muell Arg seeds. Int. J. Pharm. Phytochem. Res. 8, 386–392.

Elumalai, E., Prasad, T., Hemachandran, J., Therasa, S.V., Thirumalai, T., David, E., 2010. Extracellular synthesis of silver nanoparticles using leaves of Euphorbia hirta and their antibacterial activities. J. Pharm. Sci. Res. 2, 549–554.

Emam, M., El Raey, M.A., Eisa, W.H., El-Haddad, A.E., Osman, S.M., El-Ansari, M.A., Rabie, A.-G.M., 2017. Green synthesis of silver nanoparticles from Caesalpinia gilliesii (hook) leaves: antimicrobial activity and in vitro cytotoxic effect against bj-1 and mcf-7 cells. J. Appl. Pharm. Sci. 7, 226–233.

Fernandes, A., Sousa, A., Mateus, N., Cabral, M., De Freitas, V., 2011. Analysis of phenolic compounds in cork from quercus suber L. By hplc–dad/esi–ms. Food Chem. 125, 1398–1405.

Fischer, U.A., Carle, R., Kammerer, D.R., 2011. Identification and quantification of phenolic compounds from pomegranate (punica granatum L.) peel, mesocarp, aril and differently produced juices by hplc-dad–esi/msn. Food Chem. 127, 807–821.

Govindaraju, K., Krishnamoorthy, K., Alsagaby, S.A., Singaravelu, G., Premanathan, M., 2015. Green synthesis of silver nanoparticles for selective toxicity towards cancer cells. IET Nanobiotechnol. 9, 325–330.

Grynberg, N., Carvalho, M.D., Velandia, J., Oliveira, M., Moreira, I., Braz-Filho, R., Echevarria, A., 2002. Dna topoisomerase inhibitors: biflavonoids from ouratea species. Braz. J. Med. Biol. Res. 35, 819–822.

Hawas, U.W., 2007. Antioxidant activity of brocchlin carboxylic acid and its methyl ester from chrozophora brocchiana. Nat. Prod. Res. 21, 632–640.

He, J., Feng, Y., Ouyang, H.-Z., Yu, B., Chang, Y.-X., Pan, G.-X., Dong, G.-Y., Wang, T., Gao, X.-M., 2013. A sensitive lc–ms/ms method for simultaneous determination of six flavonoids in rat plasma: application to a pharmacokinetic study of total flavonoids from mulberry leaves. J. Pharm. Biomed. Anal. 84, 189–195.

Kalishwaralal, K., Deepak, V., Pandian, S.R.K., Kottaisamy, M., Barathmanikanth, S., Kartikeyan, B., Gurunathan, S., 2010. Biosynthesis of silver and gold nanoparticles using brevibacterium casei. Colloids Surf. Biointerf. 77, 257–262.

Kaur, R., Singh, J., Singh, G., Kaur, H., 2011. Anticancer plants: a review. J. Nat. Prod. Plant Resour. 1, 131–136.

Kavitha, S., Kovan, T.K., Bharathi, R.V., 2015. In vitro antioxidant and anticancer studies on the leaf of Acalypha indica. Biomed. Pharmacol. J. 2, 431–435.

Kuhnert, N., Jaiswal, R., Matei, M.F., Sovdat, T., Deshpande, S., 2010. How to distinguish between feruloyl quinic acids and isoferuloyl quinic acids by liquid chromatography/tandem mass spectrometry. Rapid Commun. Mass Spectrom. 24, 1575–1582.
Kumar Jain, C., Kumar Majumder, H., Roychoudhury, S., 2017. Natural compounds as anticancer agents targeting dna topoisomerases. Curr. Genom. 18, 75–92.
Laco, G.S., Collins, J.R., Luke, B.T., Kroth, H., Sayer, J.M., Jerina, D.M., Pommier, Y., 2002. Human topoisomerase I inhibition: docking camptothecin and derivatives into a structure-based active site model. Biochemistry 41, 1428–1435.
Lee, E.-J., Shin, S.-Y., Lee, J.-Y., Lee, S.-J., Kim, J.-K., Yoon, D.-Y., Woo, E.-R., Kim, Y.-M., 2012. Cytotoxic activities of amentoflavone against human breast and cervical cancers are mediated by increasing of pten expression levels due to peroxisome proliferator-activated receptor Γ activation. Bull. Korean Chem. Soc. 33, 2219–2223.
Liao, S., Ren, Q., Yang, C., Zhang, T., Li, J., Wang, X., Qu, X., Zhang, X., Zhou, Z., Zhang, Z., 2015. Liquid chromatography–tandem mass spectrometry determination and pharmacokinetic analysis of amentoflavone and its conjugated metabolites in rats. J. Agric. Food Chem. 63, 1957–1966.
López-Lázaro, M., Martín-Cordero, C., Ayuso, M.J., 2000. Two new flavonol glycosides as dna topoisomerase I poisons. Z. Naturforsch. C Biosci. 55, 898–902.
López-Lázaro, M., Martín-Cordero, C., Toro, M., Ayuso, M., 2002. Flavonoids as dna topoisomerase I poisons. J. Enzym. Inhib. Med. Chem. 17, 25–29.
Madlener, S., Svacinová, J., Kitner, M., Kopecky, J., Eytner, R., Lackner, A., Vo, T.P.N., Frisch, R., Grusch, M., De Martin, R., 2009. In vitro anti-inflammatory and anticancer activities of extracts of Acalypha alopecuroidea (Euphorbiaceae). Int. J. Oncol. 35, 881–891.
Marrez, D.A., El Raey, M.A., Ali, M., Seif, M.M., Ragab, T.I., El Negoumy, S.I., Emam, M., 2017. Phenolic profile And antimicrobial activity of green synthesized Acalypha wilkesiana seeds silver nanoparticles against some food borne pathogens. Biosci. Res. 14, 817–830.
Meyer, J., Afolayan, A., Taylor, M., Engelbrecht, L., 1996. Inhibition of herpes simplex virus type 1 By aqueous extracts from shoots of Helichrysum aureonitens (asteraceae). J. Ethnopharmacol. 52, 41–43.
Moco, S., Bino, R.J., Vorst, O., Verhoeven, H.A., De Groot, J., Van Beek, T.A., Vervoort, J., De Vos, C.R., 2006. A liquid chromatography-mass spectrometry-based metabolome database for tomato. Plant Physiol. 141, 1205–1218.
Moe 2014, 2014. Molecular Operating Environment, vol. 09 Chemical Computing Group Inc., 1010 Sherbooke St. West, Suite #910, Montreal, Qc, Canada H3a 2r7.
Pommier, Y., 2009. Dna topoisomerase I inhibitors: chemistry, biology, and interfacial inhibition. Chem. Rev. 109, 2894–2902.
Pommier, Y., 2013. Drugging topoisomerases: lessons and challenges. ACS Chem. Biol. 8, 82–95.
Pommier, Y., Leo, E., Zhang, H., Marchand, C., 2010. Dna topoisomerases and their poisoning by anticancer and antibacterial drugs. Chem. Biol. 17, 421–433.
Prayong, P., Barusrux, S., Weerapreeyakul, N., 2008. Cytotoxic activity screening of some indigenous Thai plants. Fitoterapia 79, 598–601.
Ramirez, J.E., Zambrano, R., Sepúlveda, B., Simirgiotis, M.J., 2013. Antioxidant properties and hyphenated hplc-pda-ms profiling of Chilean Pica mango fruits (mangifera indica L. Cv. Piqueño). Molecules 19, 438–458.
Rivero, P.J., Goicoechea, J., Urrutia, A., Arregui, F.J., 2013. Effect of both protective and reducing agents in the synthesis of multicolor silver nanoparticles. Nanoscale Res. Lett. 8, 101.
Safaepour, M., Shahverdi, A.R., Shahverdi, H.R., Khorramizadeh, M.R., Gohari, A.R., 2009. Green synthesis of small silver nanoparticles using geraniol and its cytotoxicity against fibrosarcoma-wehi 164. Avicenna J. Med. Biotechnol. (AJMB) 1, 111.
Santos, S.A., Villaverde, J.J., Sousa, A.F., Coelho, J.F., Neto, C.P., Silvestre, A.J., 2013. Phenolic composition and antioxidant activity of industrial cork by-products. Ind. Crops Prod. 47, 262–269.
Seng, H.-L., Tan, K.-W., Maah, M.J., Ng, S.-W., Rahman, R.N.Z.R.A., Caracelli, I., Ng, C.-H., 2010. Crystal structure, dna binding studies, nucleolytic property and topoisomerase I inhibition of zinc complex with 1, 10-phenanthroline and 3-methylpicolinic acid. Biometals 23, 99.
Shrestha, S., Park, J.-H., Lee, D.-Y., Cho, J.-G., Seo, W.-D., Kang, H.C., Yoo, K.-H., Chung, I.-S., Jeon, Y.-J., Yeon, S.-W., 2012. Cytotoxic and neuroprotective biflavonoids from the fruit of rhus parviflora. J. Kor. Soc. Appl. Biol. Chem. 55, 557–562.
Sisodiya, P.S., 2013. Plant derived anticancer agents: a review. Int. J. Res. Dev. Pharm. Life Sci. 2, 293–308.
Sivalokanathan, S., Ilayaraja, M., Balasubramanian, M., 2005. Efficacy of Terminalia Arjuna (Roxb.) on N-Nitrosodiethylamine Induced Hepatocellular Carcinoma in Rats.
Sobeh, M., Mahmoud, M.F., Abdelfattah, M.A., El-Beshbishy, H.A., El-Shazly, A.M., Wink, M., 2017. Albizia harveyi: phytochemical profiling, antioxidant, antidiabetic and hepatoprotective activities of the bark extract. Med. Chem. Res. 26, 3091–3105.
Staker, B.L., Feese, M.D., Cushman, M., Pommier, Y., Zembower, D., Stewart, L., Burgin, A.B., 2005. Structures of three classes of anticancer agents bound to the human topoisomerase I− dna covalent complex. J. Med. Chem. 48, 2336–2345.
Staker, B.L., Hjerrild, K., Feese, M.D., Behnke, C.A., Burgin, A.B., Stewart, L., 2002. The mechanism of topoisomerase I poisoning by a camptothecin analog. Proc. Natl. Acad. Sci. Unit. States Am. 99, 15387–15392.
Tanaka, T., Tong, H.-H., Xu, Y.-M., Ishimaru, K., Nonaka, G.-I., Nishioka, I., 1992. Tannins and related compounds. Cxvii. Isolation and characterization of three new ellagitannins, lagerstannins a, B and C, having a gluconic acid core, from lagerstroemia speciosa (l.) pers. Chem. Pharm. Bull. 40, 2975–2980.
Tomczyk, M., Drozdowska, D., Bielawska, A., Bielawski, K., Gudej, J., 2008. Human dna topoisomerase inhibitors from potentilla argentea and their cytotoxic effect against mcf-7. Die Pharmazie-An International Journal Of Pharmaceutical Sciences 63, 389–393.
Varadavenkatesan, T., Selvaraj, R., Vinayagam, R., 2019. Dye degradation and antibacterial activity of green synthesized silver nanoparticles using Ipomoea digitata linn. Flower extract. Int. J. Environ. Sci. Technol. 16, 2395–2404.
Vassallo, A., Vaccaro, M.C., De Tommasi, N., Dal Piaz, F., Leone, A., 2013. Identification of the plant compound geraniin as a novel Hsp90 inhibitor. PLoS One 8, E74266.
Vichai, V., Kirtikara, K., 2006. Sulforhodamine B colorimetric assay for cytotoxicity screening. Nat. Protoc. 1, 1112.
Vilar, S., Cozza, G., Moro, S., 2008. Medicinal chemistry and the molecular operating environment (moe): application of qsar and molecular docking to drug discovery. Curr. Top. Med. Chem. 8, 1555–1572.
Vinayagam, R., Varadavenkatesan, T., Selvaraj, R., 2017. Evaluation of the anticoagulant and catalytic activities of the bridelia retusa fruit extract-functionalized silver nanoparticles. J. Clust. Sci. 28, 2919–2932.
Vos, S.M., Tretter, E.M., Schmidt, B.H., Berger, J.M., 2011. All tangled up: how cells direct, manage and exploit topoisomerase function. Nat. Rev. Mol. Cell Biol. 12, 827.
Webster, G.L., 1994. Synopsis of the genera and suprageneric taxa of Euphorbiaceae. Ann. Mo. Bot. Gard. 33–144.
Xin, L.-T., Liu, L., Shao, C.-L., Yu, R.-L., Chen, F.-L., Yue, S.-J., Wang, M., Guo, Z.-L., Fan, Y.-C., Guan, H.-S., 2017. Discovery of dna topoisomerase I inhibitors with low-cytotoxicity based on virtual screening from natural products. Mar. Drugs 15, 217.
Yousuf, I., Usman, M., Ahmad, M., Tabassum, S., Arjmand, F., 2018. Single X-ray crystal structure, dft studies and topoisomerase I inhibition activity of a tailored ionic Ag (I) nalidixic acid–piperazinium drug entity specific for pancreatic cancer cells. New J. Chem. 42, 506–519.
Zayed, M.F., Eisa, W.H., Abdel-Moneam, Y.K., El-Kousy, S.M., Atia, A., 2015. Ziziphus spina-christi based bio-synthesis of Ag nanoparticles. J. Ind. Eng. Chem. 23, 50–56.
Zayed, M.F., Eisa, W.H., El-Kousy, S.M., Mleha, W.K., Kamal, N., 2019. Ficus retusa-stabilized gold and silver nanoparticles: controlled synthesis, spectroscopic characterization, and sensing properties. Spectrochim. Acta Mol. Biomol. Spectrosc. 214, 496–512.
Zayed, M.F., Eisa, W.H., Shabaka, A., 2012. Malva parviflora extract assisted green synthesis of silver nanoparticles. Spectrochim. Acta Mol. Biomol. Spectrosc. 98, 423–428.